Combined holography and thermography in a single sensor through image-plane holography at thermal infrared wavelengths

Marc P. Georges,[1,*] Jean-François Vandenrijt,[1] Cédric Thizy,[1] Igor Alexeenko,[2,4] Giancarlo Pedrini,[2] Birgit Vollheim,[3] Ion Lopez,[5] Iagoba Jorge,[5] Jonathan Rochet,[6] and Wolfgang Osten[2]

[1]*Centre Spatial de Liège, Université de Liège, Liege Science Park, B-4031 Angleur (Liege), France*
[2]*Institut für Technische Optik, Universität Stuttgart, Pfaffenwaldring 9, D-70569, Stuttgart, Germany*
[3]*InfraTec GmbH, Gostritzer Str. 61-63, D-01217 Dresden, Germany*
[4]*Immanuel Kant Baltic Federal University, A.Nevskogo str. 14, 236041, Kaliningrad, Russia*
[5]*Centro de Tecnologías Aeronáuticas, Parque Tecnológico de Álava, C/Juan de la Cierva 1, Miñano (Álava) 01510, Spain*
[6]*Optrion, Pôle d'Ingénierie des Matériaux de Wallonie, Boulevard de Colonster 4, B-4000 Liège, Belgium*
[*]*mgeorges@ulg.ac.be*

Abstract: Holographic interferometry in the thermal wavelengths range, combining a CO_2 laser and digital hologram recording with a microbolometer array based camera, allows simultaneously capturing temperature and surface shape information about objects. This is due to the fact that the holograms are affected by the thermal background emitted by objects at room temperature. We explain the setup and the processing of data which allows decoupling the two types of information. This natural data fusion can be advantageously used in a variety of nondestructive testing applications.

OCIS codes: (120.6165) Speckle interferometry, metrology; (090.1995) Digital holography; (120.6780) Temperature; (120.4290) Nondestructive testing; (140.3470) Lasers, carbon dioxide; (040.6808) Thermal (uncooled) IR detectors, arrays and imaging.

References and links

1. T. Kreis, *Handbook of Holographic Interferometry:Optical and Digital Methods* (Wiley, 2005).
2. X. Maldague, *Theory and Practice of Infrared Technology for Nondestructive Testing* (Wiley-Interscience, 2001).
3. D. Burleigh, "Portable combined thermography/shearography NDT system for inspecting large composite structures," Proc. SPIE **4710**, 578–587 (2002).
4. M. Feligiotti, E. Hack, G. Lampeas, T. Siebert, A. Pipino, and A. Ihle, "Assessment of impact damage in CFRP by combined thermal and speckle methods," Proc. SPIE **7387**, 73870H (2010).
5. S. Sfarra, C. Ibarra-Castanedo, C. Santulli, F. Sarasini, D. Ambrosini, D. Paoletti, and X. Maldague, "Eco-friendly laminates: From the indentation to non-destructive evaluation by optical and infrared monitoring techniques," Strain **49**(2), 175–189 (2013).
6. S. Sfarra, P. Theodorakeas, C. Ibarra-Castanedo, N. P. Avdelidis, A. Paoletti, D. Paoletti, K. Hrissagis, A. Bendada, M. Koui, and X. Maldague, "Evaluation of defects in panel paintings using infrared, optical and ultrasonic techniques," Insight **54**(1), 21–27 (2012).
7. M. P. Georges, J.-F. Vandenrijt, C. Thizy, Y. Stockman, P. Queeckers, F. Dubois, and D. Doyle, "Digital holographic interferometry with CO_2 lasers and diffuse illumination applied to large space reflector metrology [Invited]," Appl. Opt. **52**(1), A102–A116 (2013).
8. O. J. Løkberg and O. Kwon, "Electronic speckle pattern interferometry using a CO_2 laser," Opt. Laser Technol. **16**(4), 187–192 (1984).
9. E. Allaria, S. Brugioni, S. De Nicola, P. Ferraro, S. Grilli, and R. Meucci, "Digital holography at 10.6 μm," Opt. Commun. **215**(4-6), 257–262 (2003).
10. M. Paturzo, A. Pelagotti, A. Finizio, L. Miccio, M. Locatelli, A. Gertrude, P. Poggi, R. Meucci, and P. Ferraro, "Optical reconstruction of digital holograms recorded at 10.6 microm: route for 3D imaging at long infrared wavelengths," Opt. Lett. **35**(12), 2112–2114 (2010).

#222130 - $15.00 USD Received 1 Sep 2014; revised 6 Oct 2014; accepted 7 Oct 2014; published 13 Oct 2014

11. M. Locatelli, E. Pugliese, M. Paturzo, V. Bianco, A. Finizio, A. Pelagotti, P. Poggi, L. Miccio, R. Meucci, and P. Ferraro, "Imaging live humans through smoke and flames using far-infrared digital holography," Opt. Express **21**(5), 5379–5390 (2013).
12. J.-F. Vandenrijt and M. Georges, "Infrared electronic speckle pattern interferometry at 10 µm," Proc. SPIE **6616**, 66162Q (2007).
13. J.-F. Vandenrijt and M. P. Georges, "Electronic speckle pattern interferometry and digital holographic interferometry with microbolometer arrays at 10.6 µm," Appl. Opt. **49**, 5067–5075 (2010).
14. J.-F. Vandenrijt, C. Thizy, P. Queeckers, F. Dubois, D. Doyle, and M. P. Georges, "Long-wave infrared digital holographic interferometry with diffuser or point source illuminations for measuring deformations of aspheric mirrors," Opt. Eng. **53**(11), 112309 (2014).
15. M. P. Georges, J.-F. Vandenrijt, C. Thizy, Y. Stockman, P. Queeckers, F. Dubois, and D. Doyle, "Digital holographic interferometry with CO_2 laser applied to aspheric space reflector testing," in *Digital Holography and Three-Dimensional Imaging*, OSA Technical Digest (online) (Optical Society of America, 2013), DW3A.4.
16. I. Alexeenko, J.-F. Vandenrijt, M. P. Georges, G. Pedrini, T. Cédric, W. Osten, and B. Vollheim, "Digital holographic interferometry by using long wave infrared radiation (CO_2 laser)," Appl. Mech. Mater. **24–25**, 147–152 (2010).
17. I. Alexeenko, J.-F. Vandenrijt, G. Pedrini, C. Thizy, B. Vollheim, W. Osten, and M. P. Georges, "Nondestructive testing by using long-wave infrared interferometric techniques with CO_2 lasers and microbolometer arrays," Appl. Opt. **52**(1), A56–A67 (2013).
18. J.-F. Vandenrijt, C. Thizy, I. Alexeenko, G. Pedrini, J. Rochet, B. Vollheim, I. Jorge, P. Venegas, I. Lopez, W. Osten, and M. P. Georges, "Mobile speckle interferometer in the long-wave infrared for aeronautical nondestructive testing in field conditions," Opt. Eng. **52**(10), 101903 (2013).
19. M. H. De la Torre Ibarra, J. M. Flores Moreno, D. D. Aguayo, M. S. Hernández-Montes, C. Pérez-López, and F. Mendoza-Santoyo, "Displacement measurements over a square meter area using digital holographic interferometry," Opt. Eng. **53**(9), 092009 (2014).
20. M. Karray, P. Slangen, and P. Picart, "Comparison between digital Fresnel holography and digital image-plane holography: the role of imaging aperture," Exp. Mech. **52**(9), 1275–1286 (2012).
21. P. Slangen, M. Karray, and P. Picart, "Some figures of merit so as to compare digital Fresnel holography and speckle interferometry," Proc. SPIE **8082**, 808205 (2011).
22. J.-F. Vandenrijt, C. Thizy, I. Alexeenko, I. Jorge, I. Lopez, I. S. De Ocariz, G. Pedrini, W. Osten, and M. Georges, "Electronic speckle pattern interferometry at long infrared wavelengths. Scattering requirements," in *Fringe 2009- 6th International Workshop on Advanced Optical Metrology*, 596–599 (2009).
23. M. Ravaro, M. Locatelli, E. Pugliese, I. Di Leo, M. Siciliani de Cumis, F. D'Amato, P. Poggi, L. Consolino, R. Meucci, P. Ferraro, and P. De Natale, "Mid-infrared digital holography and holographic interferometry with a tunable quantum cascade laser," Opt. Lett. **39**(16), 4843–4846 (2014).

1. Introduction

Holographic interferometry (HI) and electronic speckle pattern interferometry (ESPI) [1] are well-known nondestructive techniques used for the full-field contactless measurement of object surface displacements, which can be determined through fringes patterns (interferograms) superimposed to the object image. Thermography is an imaging technique which is used in a wide variety of applications, among which nondestructive testing [2]. Following Planck's law, the spectral radiance of a blackbody is function of the temperature of the latter [2]. In thermography a thermal imager integrates this spectral radiance over some infrared spectral range and in a given solid angle. The resulting flux is related to the temperature of the object or scene observed. HI/ESPI and thermography are often used in combination because they give complementary information, mainly in the field of defect detection [3–6]. Nevertheless in such cases, separate devices with their own imaging systems are used in combination. Deformation map (from interferograms) and thermal images require to be resampled for correlating or comparing both.

The concept presented in this paper is based on the fact that HI or ESPI in the infrared range offers the possibility of a natural fusion of information. Indeed in the infrared these techniques use imagers which are also used in thermography. Therefore it makes sense to think capturing both information simultaneously on every pixel, which allows a perfect correlation between thermal and deformation fields.

We consider here the long-wave infrared range (LWIR) with wavelengths between 8 and 14 micrometers and the CO_2 laser as coherent source, with various possible lines around 10 micrometers. Photochemical hologram recording at this wavelength was studied already in the 1960s years. In a previous paper [7] we performed a literature survey of the different

#222130 - $15.00 USD Received 1 Sep 2014; revised 6 Oct 2014; accepted 7 Oct 2014; published 13 Oct 2014

materials. We showed that there was no convincing material for recording holograms to be used in HI, mainly because of low resolution and some other practical considerations. Therefore electronic hologram recording is preferred due to the recent development of various thermal focal plane array technologies, which is in constant evolution in terms of performances and resolution.

The very first evidence of such LWIR electronic recording was provided by Løkberg and Kwon in 1984 [8] which showed ESPI with CO_2 lasers associated with pyroelectric vidicon cameras. The vidicon image capture requires variable image intensity. Therefore only variating speckle patterns could be recorded which limited the application of ESPI on vibrating objects. In 2003 Allaria *et al.* [9] proposed LWIR digital holography (DH) with a modified pyroelectric sensor array which allows imaging of static objects. Since then that group showed numerous applications and advantages of LWIR DH. One advantage of LWIR DH is the possibility of reconstructing numerically objects larger than in visible DH (for a given distance between the object and the sensor) because the ratio of the wavelength and pixel size is generally 5 to 10 times larger in LWIR [7,10]. Recently it was demonstrated that lensless LWIR DH can capture laser light reflected by humans illuminated through smokes and flames and reconstruct numerically images of sufficient quality to recognize the presence of people located beyond [11].

In the metrology and nondestructive testing domain, we have shown various developments and applications. Our preliminary LWIR ESPI results concerned in-plane ESPI [12], out-of-plane ESPI [13] and out-of-plane lensless digital holographic interferometry (DHI) [13]. In these methods one observes the optical phase differences that are related to the object displacement or deformation between two object states. The advantages of LWIR are the displacement measurement range which is 20 times larger in the LWIR than in the visible and the relaxed stability constraints [12,13]. We pursued these studies by the development of LWIR DHI for the deformation metrology of large aspheric space reflectors under space simulated environment [7], with various types of illuminations for dealing with the specularity of surfaces [14] and we have demonstrated its application to exotic shapes like off-axis elliptic reflectors [15].

The work presented here is related to developments in LWIR digital holography in view of nondestructive testing of aeronautical composites. We already showed achievements of LWIR DHI [16] and comparison of different LWIR interferometric techniques and optimization of an ESPI setup [17]. These works resulted in the development of a mobile ESPI head which included the CO_2 laser and a thermographic camera based on a microbolometers array. We demonstrated that the use of such long infrared wavelengths allows working in nondestructive testing applications in industrial environment. In particular large composite structures were examined in hangar conditions [18]. The nondestructive testing of large structures in industrial environments is a hot topic and various works propose alternative solutions to LWIR ESPI [19].

The present paper is a continuation of previous ones and we demonstrate for the first time to the best of our knowledge that LWIR digital holography allows simultaneous recording of the surface shape and temperature. Indeed the thermal background is incoherent by nature, thus only the information coming from the laser illumination and related to the object surface shape can be numerically reconstructed by DH. For that reason we need to consider image-plane DH or classical ESPI configurations for which the focus of the object (including its thermal background) is insured by the objective lens put in front of the thermographic camera.

We will recall first the basic principle of digital holography and describe the combination of temperature and deformation measurement. Then we describe the set-up and present a series of applications, from the thermo-mechanical measurements on composites to defect detection performed on-site.

#222130 - $15.00 USD Received 1 Sep 2014; revised 6 Oct 2014; accepted 7 Oct 2014; published 13 Oct 2014

2. Combination of shape and temperature measurements

Digital hologram recording consists in illuminating an object with a laser and realize interference between the object and reference beams on a camera array. Their interference produces, at instant t and in every pixel (x, y), an intensity pattern $I_H(x, y)$ given by

$$I_H(x,y,t) = I_R(x,y,t) + I_O(x,y,t) + 2\sqrt{I_R(x,y,t).I_O(x,y,t)}\cos\left(\phi(x,y,t)\right), \quad (1)$$

where $I_R(x,y,t)$ and $I_O(x,y,t)$ are respectively the intensities of the reference and object beams at the sensor level, the phase $\phi(x,y,t) = \varphi_R(x,y,t) - \varphi_O(x,y,t)$ is the difference of $\varphi_R(x,y,t)$ and $\varphi_O(x,y,t)$ which are respectively the phases of the reference and object beams. We have omitted in (1) the contributions of incoherent noise sources and which would have added an intensity term on the right-hand side.

When holographic recording is applied at thermal wavelengths, the total intensity pattern of the hologram can be expressed as the superposition of the interference pattern $I_H(x,y,t)$ given by (1), and an incoherent thermal background term $I_{Th}(x,y,t)$:

$$I(x,y,t) = I_H(x,y,t) + I_{Th}(x,y,t). \quad (2)$$

Our aim is to obtain a simultaneous image of the object thermal background (so-called thermogram) and a recording of the phase, moreover in every pixel (x, y) . In order to produce such a thermal image, we cannot use a lensless DH recording configuration. Indeed the thermal background being incoherent, it cannot be reconstructed and propagated at an arbitrary distance through the usual DH reconstruction principle. Conversely, by using an image-plane holographic configuration, the image is focused optically by a lens onto the camera array. Such digital image-plane holography has been compared to lensless classical DH [20]. In the case of perfect focusing by an optical device, it is similar to ESPI which can be seen as a particular configuration of DH as stated by Slangen *et al.* [21]. Indeed ESPI is an in-line image-plane DH configuration and its processing is specific and involves phase-shifting, as we will see later. In these imaging conditions the intensity I_{Th} represents the emitted radiation related to the temperature of the surface of the object which is imaged on the camera sensor array.

The combination principle is depicted in Fig. 1: Fig. 1(a) shows a typical simulated holographic pattern recorded at thermal wavelength, Fig. 1(b) shows the thermogram that would be recorded if the thermographic camera was used without the laser. When the holographic part of the setup is used (i.e. the laser beam is present), the interference pattern is a high spatial frequency pattern represented in Fig. 1(c). Figure 1(d) shows the profiles of both thermal and interference components on a line y = Y, respectively the red and blue plots.

#222130 - $15.00 USD Received 1 Sep 2014; revised 6 Oct 2014; accepted 7 Oct 2014; published 13 Oct 2014

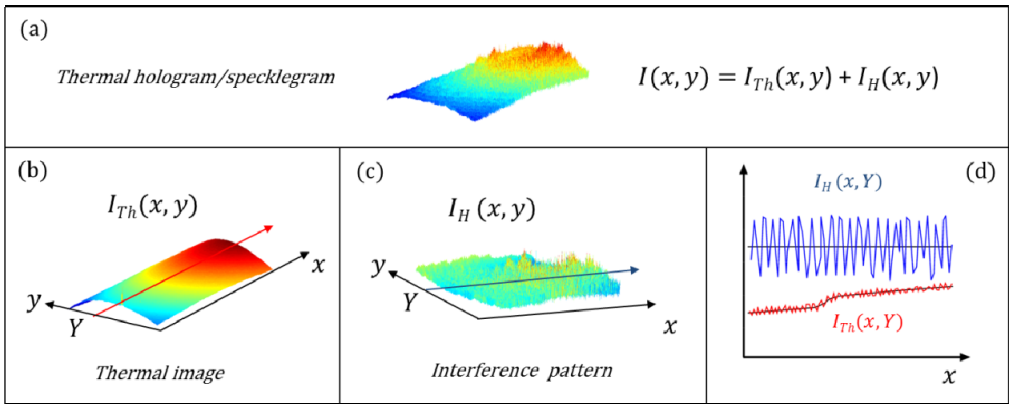

Fig. 1. Principle of combination: (a) hologram or specklegram recorded at thermal wavelengths, (b) thermal part of the former, (c) interference part of the former, (d) line profile along line y = Y.

The next section is devoted to the LWIR holographic set-up which was developed for the proposed technique.

3. Set-up

In previous papers we already have shown various LWIR holographic set-ups in view of a transportable system [17]. The objective lens (OL) is preferably not detached from the camera housing for different reasons explained by Alexeenko *et al.* [17]. This imposes to bring the reference beam through the entrance face of the objective lens. This is not the case in the holographic set-up in the visible, where the reference beam is brought through a beam combiner placed between the camera array and the OL. In LWIR a beam combiner is placed in front. Figure 2 shows the arrangement which has been used for a mobile LWIR holographic set-up developed for nondestructive testing in field conditions [18]. The setup is first composed of an upper bench (Fig. 2(a)) with the camera and its OL, a beam combiner (BC), a folding mirror mounted on a stage with a piezoelectric element (MPZT), a diverging lens (L) and a concave mirror (CM) which reflects the reference beam (RB) backwards to the camera. The camera is a VarioCAM hr from Jenoptik, with 640 x 480 pixels of 25 x 25 square micrometers size (giving a detector size of 16 x 12 square millimeters), a dynamic range of 16 bits and a frame rate of 50 frames per second, running with IRBIS software by Infratec GmbH. The OL of the camera module has a 50 millimeters focal length, is made of Germanium and is especially designed for thermography in order to provide maximal resolution and field-of-view. Working distances used are on the order of 1 meter, which gives an observed area typically 25 centimeters wide with the 50 millimeters focal length. The other part of the setup is constituted by a lower bench containing mainly the CO_2 laser. The latter is the Merit-S, emitting at a wavelength of 9.3 µm, with a maximum output power of 8 W, and manufactured by Access Laser Co. Its coherence length is not known from the manufacturer but CO_2 lasers have linewidths of a few tens of kHz which insures coherence lengths larger than meters or tens of meters and is highly comfortable for holography. However an important issue for using CO_2 lasers in holographic interferometry is to avoid mode hop which is a known problem for such lasers and that generates unwanted wavelength changes during measurements. For that reason water pipes (WP), connecting the laser to a chiller device, are necessary for stabilizing the laser temperature during operations, insuring a stable emission line. Other elements of the lower bench are folding mirrors (M1, M2, and M3), a shutter (SH) and a polarizing beamsplitter (PBS). The latter allows separating the laser beam in two parts: the object beam (OB) and the reference beam (RB, dashed line). Figure 2(c) shows the details of the PBS (manufactured by II-VI Infrared) consisting of two stacks of

#222130 - $15.00 USD Received 1 Sep 2014; revised 6 Oct 2014; accepted 7 Oct 2014; published 13 Oct 2014

three ZnSe plates placed in chevron geometry, with each plate working at Brewster angle. Such assembly transmits the *p*-polarization and reflects the *s*-polarization. The *p*-polarized beam constitutes the object illumination beam and travels to the object via two folding mirrors M3 and M4 and the illumination lens (IL). The reference beam (*s*-polarized) travels from the lower to the upper bench and reaches lens L. Figure 2(d) shows a picture of the mobile instrument.

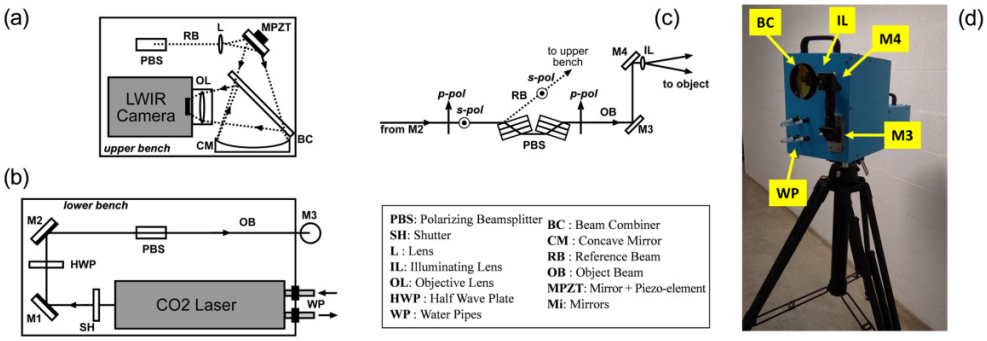

Fig. 2. Mobile LWIR holographic setup: schemes of (a) upper bench with camera, (b) lower bench, (c) beam separation assembly; (d) picture of the instrument.

One important requirement for the instrument was that the thermal background must not be disturbed, or the less possible, by the holographic part of the setup. With respect to this, the most problematic element is the beamsplitter used as BC. Indeed if we choose for example a beamsplitter with a reflectance of 50% and transmittance 50% (R50/T50) over the entire LWIR spectrum, this means that only half of the object thermal radiation will reach the camera. This in turn would strongly increase the uncertainty on the surface temperature measurement. For overcoming this, a specific BS had to be developed for the application. LWIR beamsplitters are made of coatings on ZnSe substrate. We specified the coating to be most transmitting over the LWIR spectrum and the less reflecting on the same extent, except for the laser wavelength, say around 10 µm. An ideal BC should have a 100% reflectance at the laser wavelength and 0% elsewhere. The BC was built by II-VI Company and the most suitable coating that was obtained for us has the spectral properties shown in Fig. 3 (these graphs are the computed values provided by the manufacturer, not actual measured ones).

#222130 - $15.00 USD Received 1 Sep 2014; revised 6 Oct 2014; accepted 7 Oct 2014; published 13 Oct 2014

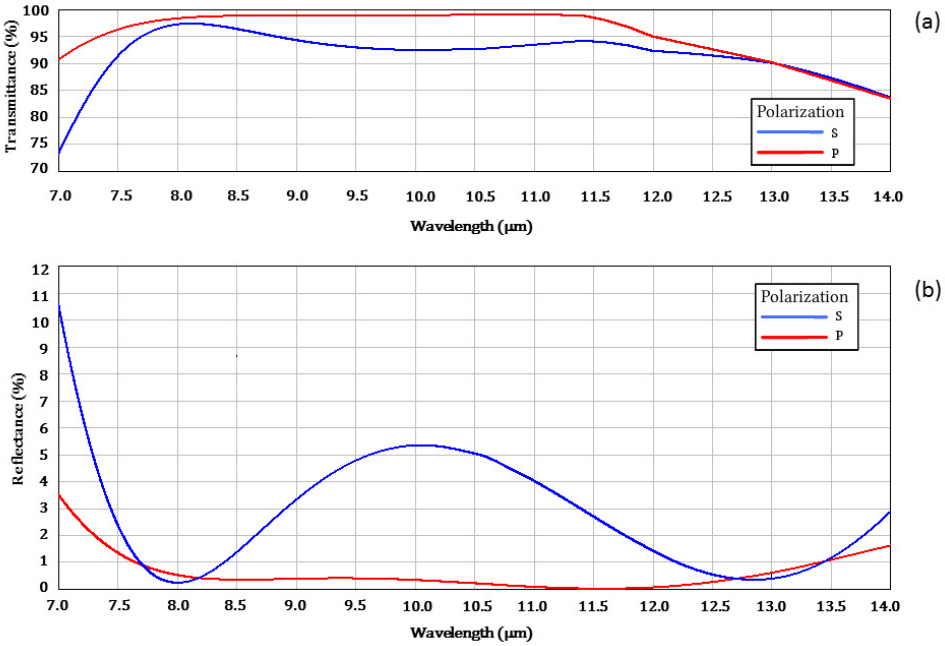

Fig. 3. Spectral properties of the beam combiner for s- and p-polarizations: (a) transmittance, (b) reflectance.

Since the thermal background is not polarized, the global transmittance is a combination of both *s* and *p* ones and the loss will remain limited to a few percents. This impacts the infrared irradiance on the camera array, i.e. $I_{Th}(x,y,t)$, hence the temperature measurement. Temperature measurement assumes a calibration process, e.g. by using a blackbody at a precise temperature. The camera has been calibrated in factory prior delivery. A proper calibration could have been performed with the BC. However we have not considered such recalibration here. Indeed in our nondestructive testing applications, only temperature variations are needed and not the actual temperature. Therefore we will not pay attention to the small transmittance loss which will be considered as almost constant between two close temperatures.

The users generally require that the temperature variations and deformations are measured during a specific load and that both are provided in separate data sets. One important part of the work was then to find procedure(s) allowing a separation of the two components contained in the intensity (2) at several instants during loading of the object monitored. Therefore we need to compute, on the one hand, the difference of the thermograms $I_{Th}(x,y,t_i)$ captured at different instants t_i and, on the other hand, the difference of phases $\phi(x,y,t_i)$ contained in the interference term of (1). The latter will lead us to consider quantification of phase methods, in particular the phase-shifting technique. In the following section we present some procedures for separating the two signals.

4. Separation of signals

The separation method is based on the phase-shifting. The phase of the object state can be calculated through the phase-shifting process [1] which is recalled hereafter. This situation is depicted in Fig. 4. Let us call t_a, t_b, t_c,… different instants at which one wants to record the

#222130 - $15.00 USD Received 1 Sep 2014; revised 6 Oct 2014; accepted 7 Oct 2014; published 13 Oct 2014

temperature and shape state of the evolving object. During the acquisition of the intensity patterns (2) the camera is synchronized with the piezo-element which moves the mirror MPZT in the reference beam and a sequence of *n* phase-shifted intensity patterns $\{I(t_a)\}$ is recorded at instant t_a, a second similar sequence $\{I(t_b)\}$ is recorded at instant t_b, and so on. The duration of one sequence is limited by the stepped movement of the MPZT which is set to 100 ms per step, giving an overall duration of typically 400 ms, considering the 20 ms recording time for each frame.

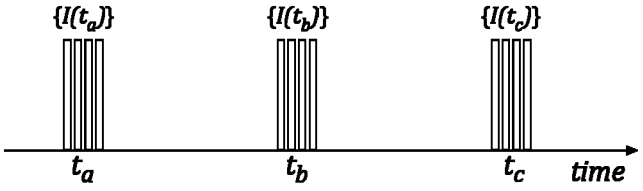

Fig. 4. Typical temporal sequence of operations for simultaneous thermogram measurement.

In our case we apply the 4-bucket algorithm which consists of acquiring a set of four holograms/specklegrams with a π/2 phase shift between each acquisition. Let us suppose that neither the reference and object beam intensities, resp. $I_{R,a}$ and $I_{O,a}$, nor the thermogram $I_{Th,a}$ and the phase ϕ_a have varied during the sequence at time t_a. We can write, omitting the (x, y) dependency for simplicity, that the n^{th} image of the sequence is:

$$I_n(t_a) \equiv I_{a,n} = I_{Th,a} + I_{R,a} + I_{O,a} + 2\sqrt{I_{R,a}\, I_{O,a}}\cos\left(\phi_a + (n-1)\frac{\pi}{2}\right), \tag{3}$$

with n = 1,2,3,4. The phase is computed as [1]

$$\phi_a = \tan^{-1}\left[\left(I_{a,4} - I_{a,2}\right)/\left(I_{a,1} - I_{a,3}\right)\right]. \tag{4}$$

The determination of the thermogram $I_{Th,a}$ could be deduced by substituting the phase calculated by (4) into (3) and knowing one of the measurement $I_{a,n}$ as well as preliminary recording of $I_{R,a}$ and $I_{O,a}$. However a simpler way is to compute the sum of the 4 phase-shifted intensities $I_{a,1}$, $I_{a,2}$, $I_{a,3}$ and $I_{a,4}$ and it comes

$$I_{Th,a} = \frac{1}{4}\left(I_{1,a} + I_{2,a} + I_{3,a} + I_{4,a}\right) - I_{R,a} - I_{O,a}. \tag{5}$$

It is then sufficient to record preliminary separate beam intensities $I_{R,a}$ and $I_{O,a}$ for solving (5).

At a subsequent moment t_b a new sequence of 4 phase-shifted intensity patterns $\{I(t_b)\}$ is captured. The phase ϕ_b can be computed similarly to ϕ_a. The quantity of interest in the application is the phase difference $\Delta\phi = \phi_a - \phi_b$ which is related to the displacement **d** of each object point, imaged in each point of the camera (x, y). This relationship is given by [1]:

$$\Delta\phi = \frac{2\pi}{\lambda}\mathbf{s}.\mathbf{d}, \tag{6}$$

where the sensitivity vector defined by $\mathbf{s} = \mathbf{k}_1 - \mathbf{k}_2$ is determined by the geometry of the set-up, $\mathbf{k}_1$ and $\mathbf{k}_2$ are the unit vectors of illumination and observation respectively. In our case,

#222130 - $15.00 USD Received 1 Sep 2014; revised 6 Oct 2014; accepted 7 Oct 2014; published 13 Oct 2014

the object is globally perpendicular to the observation and illumination directions. As a result the displacement **d** is out-of-plane.

The thermogram difference is simply obtained by

$$\Delta I_{Th} = \frac{1}{4}\left[\sum_{i=1}^{4} I_{i,a} - \sum_{i=1}^{4} I_{i,b}\right] - \Delta I_R - \Delta I_O, \tag{7}$$

where $\Delta I_R = I_{R,a} - I_{R,b}$ and $\Delta I_O = I_{O,a} - I_{O,b}$.

In practice we consider the case where the reference and object beams intensities have not varied ($\Delta I_R = \Delta I_O = 0$), what simplifies the procedure in omitting preliminary recordings of separate beams intensities.

$$\Delta I_{Th}^{(r)} = \frac{1}{4}\left[\sum_{i=1}^{4} I_{i,a} - \sum_{i=1}^{4} I_{i,b}\right]. \tag{8}$$

However if the intensities of the beams varies between t_a and t_b, an error on ΔI_{Th}, hence on temperature variation, will occur. In order to avoid this, an alternative procedure can be followed and is explained hereafter.

For cases where the phenomena observed are slow, we can consider the recording of a thermogram preliminarily to the recording of the interference pattern, as is shown in Fig. 5 which represents the temporal sequence of operations. We need a shutter at the laser output which is closed prior to this preliminary acquisition (red rectangle). Then the thermogram $I_{Th}(t_a)$ is captured (first white rectangle). Shortly after the shutter is opened (green rectangle) and a sequence of 4 phase-shifted intensity patterns $\{I(t_a)\}$ is recorded. The duration of one sequence is typically 500 ms, considering the MPZT stepped movement, the duration of the different frames captures and the shutter operation.

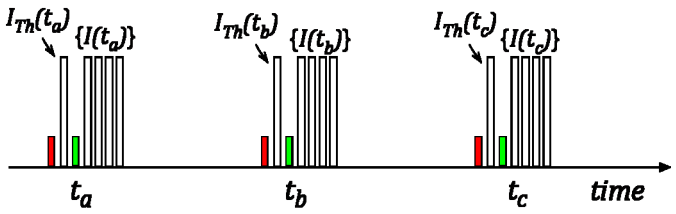

Fig. 5. Typical temporal sequence of operations for separate initial thermogram measurement.

At a subsequent moment t_b a new sequence of 4 phase-shifted intensity patterns $\{I(t_b)\}$ is captured, with a preliminary thermogram recording $I_{Th}(t_b)$, as depicted in Fig. 5. In this procedure, the temperature variation is simply obtained by subtracting the preliminary thermograms captured at the beginning of each sequence:

$$\Delta I_{Th}^{(p)} = I_{Th}(t_a) - I_{Th}(t_b). \tag{9}$$

We designate it by $\Delta I_{Th}^{(p)}$ to not confuse it with (9), where $\Delta I_{Th}^{(r)}$ is obtained by reconstruction from the phase-shifting approach. The computing of (9) is much simpler than (8) and $\Delta I_{Th}^{(p)}$ is not subject to potential errors related to the assumption $\Delta I_R = \Delta I_O = 0$ which led to (8).

In the next section devoted to results, we will present a series of phase maps $\Delta\phi(x,y)$ and temperature variations $\Delta I_{Th}(x,y)$ which were obtained when composite samples undergo thermal loads.

#222130 - $15.00 USD Received 1 Sep 2014; revised 6 Oct 2014; accepted 7 Oct 2014; published 13 Oct 2014

5. Results

We have applied the procedure explained above to various applications. The first example uses a sample shown in Fig. 6(a) and which consists of a helicopter panel constituted by sandwich made of honeycomb and carbon fiber reinforced polymer (CFRP) skins. The sample had a circular repair in its center and the zone observed (22 × 18 cm^2) is marked by a rectangle in red dots. The sample was not covered with any scattering removable powder, as is sometimes the case in holography. Indeed the roughness was sufficiently high and close to the wavelength that we were able to generate speckle from the surface itself, as is sometimes the case with CFRP composites [22]. A typical interference pattern between the reference and object beams is shown in Fig. 6(b).

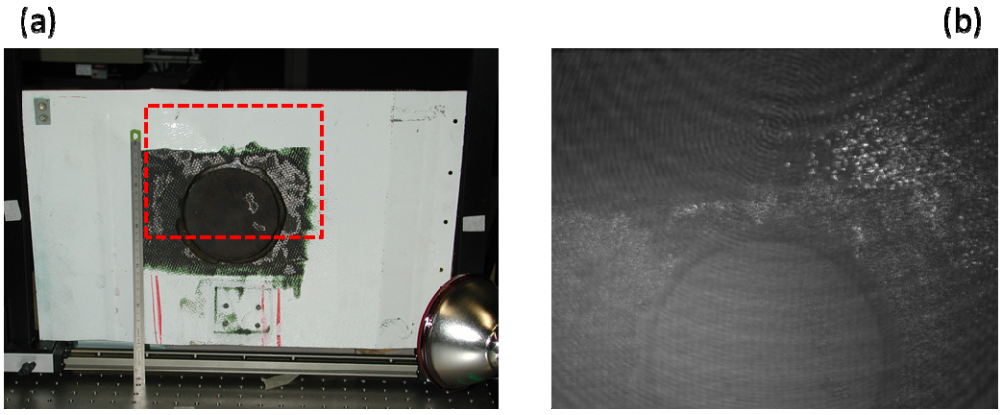

Fig. 6. (a) Sandwich panel with circular repair in the centre. The zone observed in marked by red dots. (b) Interference between reference and object beams.

The sample is heated by a halogen lamp placed at a certain angle for not blocking the field-of-view, as shown in Fig. 6(a). Figure 7(a) shows the temperature variation $\Delta I_{Th}^{(p)}$ obtained by the alternative approach explained in the previous section (see Fig. 5), while Fig. 7(b) shows the temperature $\Delta I_{Th}^{(r)}$ obtained by reconstructing the thermograms through the phase-shifting (see Fig. 4). The blue color represents the lower temperature variations, whereas the red color represents the higher ones. Figure 7(c) shows the phase variation modulo 2π obtained by calculation of (4) for two different object states and computing the phase difference $\Delta\phi$. This allows obtaining the out-of-plane displacement d through (6) after phase unwrapping, as can be seen in Fig. 7(d). Figure 7(e) shows a hybrid representation consisting of the 3D plot of the deformation which is colored with the temperature difference value obtained in each pixel. This example illustrates well the potentiality of our technique which allows obtaining both types of information in every pixel and simultaneously or quasi-simultaneously depending on the procedure followed.

#222130 - $15.00 USD Received 1 Sep 2014; revised 6 Oct 2014; accepted 7 Oct 2014; published 13 Oct 2014

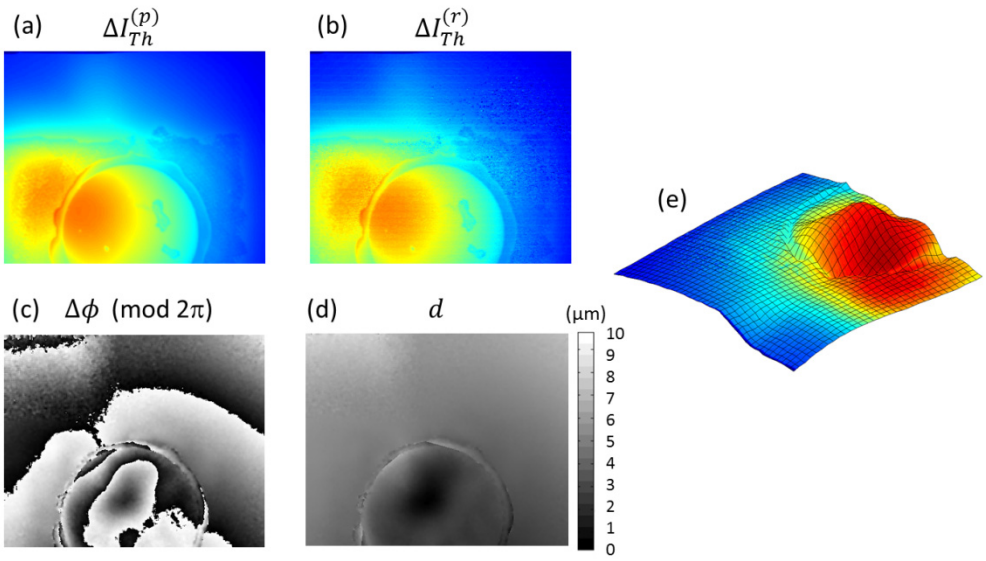

Fig. 7. (a) Temperature variation obtained by preliminary thermogram capture, (b) temperature variation obtained by reconstruction through the phase-shifting approach, (c) phase variation (modulo 2π), (d) grey level deformation map corresponding to (c), (e) hybrid representation of the deformation and temperature variation.

It can be seen that some noise is present in the reconstructed thermograms $\Delta I_{Th}^{(r)}$, (Fig. 7(b)). This noise looks like speckle and is probably due to the variation of laser beam irradiances during the phase-shifting process. For that reason we prefer the preliminary capture approach (Fig. 7(a)) which provides better quality results. Nevertheless in this case we don't have the perfect simultaneity between temperature and deformation.

The resolution in deformation measurements was already discussed in previous papers and we found typical values of 1 µm [13]. Concerning temperature, with the Jenoptik VarioCAM hr camera of our combined system, the manufacturer announces a thermal resolution better than 30 mK and an accuracy of +/– 1.5 mK. In the case of the procedure with preliminary thermogram measurement (Fig. 5), we consider that these are the performances of our system in term of temperature measurement capabilities, although affected by a few percent due to the beam combiner, as already mentioned. In terms of temperature variations measurement, we double these measurement errors since we have two measurements. By taking linear profiles in Fig. 7(a) and Fig. 7(b), we have found typical 5% variations between both methods. However in the case of the temperature variation determination, we rely on $\Delta I_{Th}^{(r)}$ which is affected by any potential variations of reference and object beam irradiances between two sequences (see Eq. (7) and which are difficult to predict.

Another experiment was settled to show the advantage of the combined system with respect to separate ones. The application consists of measuring the deformation of three CFRP coupons which are heated at gradually increasing temperature steps. One coupon is made only of CFRP, both others have an additional metallic layer. The coupons are set on a Copper baseplate (Fig. 8(a)) which can be heated from ambient temperature up to 150°C. The heat is transferred to the sample mainly by conduction. Conducting grease is also applied to improve contact and help further conduction. Such high temperatures usually prevent performing holographic or speckle interferometry in the visible, due to the air turbulences. In LWIR we are less sensitive to displacements measured, as well as perturbations of the environment. For further limiting the effect of turbulences, the baseplate is set almost

#222130 - $15.00 USD Received 1 Sep 2014; revised 6 Oct 2014; accepted 7 Oct 2014; published 13 Oct 2014

vertically (Fig. 8(b)) and the coupons are kept in place on the baseplate by two screws on which they are simply in contact. The coupons are allowed to expand freely under the effect of heating. Contrarily to the previous example, the coupons and the baseplate were sprayed with a removable scattering powder (not shown on the figure). Indeed the baseplate was highly specular, which could cause potential damages to the microbolometer array from back reflections of the laser illumination [13]. This experiment was requested by an industrial composite manufacturer who required measurement of deformation by dimensional measurement (by fringe projection) and local temperature (by thermocouples) at different temperature steps. This was the ideal case to test the interest of our combined technique. Figure 8(b) shows the dimensional measurement system which is the ATOS sensor manufactured by the company GOM. It allows measuring the coordinate of surface points with an out-of-plane resolution here of 10 µm (depends on the volume measured), while our technique has a typical 1 µm resolution [13] (one tenth of the wavelength). A calibration of the temperature measurement on the sample was made in a preliminary experiment, by thermocouples. We added a counter-measurement with thermographic camera, which allowed observing the temperature homogeneity of the sample. The additional thermographic camera is a FLIR Infracam (based on microbolometer array with 120 × 120 pixels) and it is shown in Fig. 8(b).

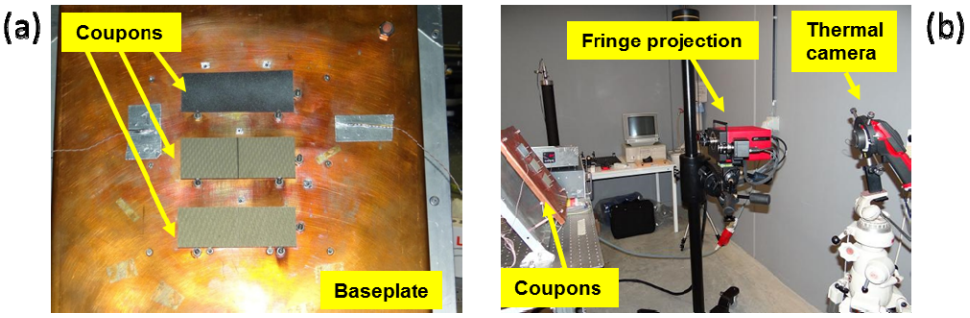

Fig. 8. (a) Heating baseplate with three coupons. (b) Setup with separate measurement techniques for deformation through dimensional measurement by fringe projection and temperature by thermographic camera.

Figure 9 shows the comparison of measurements performed by the separate techniques and those obtained by the combined one. Figure 9(a) is the out-of-plane deformation computed by the GOM ATOS software, after capture of the coordinates of surface points at two different temperatures. The amplitude of deformation is coded in color. Figure 9(b) shows the full-field temperature of a coupon obtained with the FLIR Infracam camera. Both systems have their own characteristics (magnification, lateral resolution,…), they observe the same scene at different viewing angles, and data formats are different. In order to correlate both types of data, complicated data fusion is needed. Figure 9(c) and Fig. 9(d) show respectively the phase maps (modulo 2π) and temperature variations obtained by our combined technique on the three coupons, where the baseplate has been masked out. Figure 9(e) shows a hybrid image consisting in the superposition of both data, with the baseplate visible (that way the baseplate behavior can also be taken into account if necessary).

It can be easily seen from this example the gain of the combined technique in term of correlation both in space and time of the deformation and temperature variation measurements. Moreover only one measurement system has to be set up instead of two.

#222130 - $15.00 USD Received 1 Sep 2014; revised 6 Oct 2014; accepted 7 Oct 2014; published 13 Oct 2014

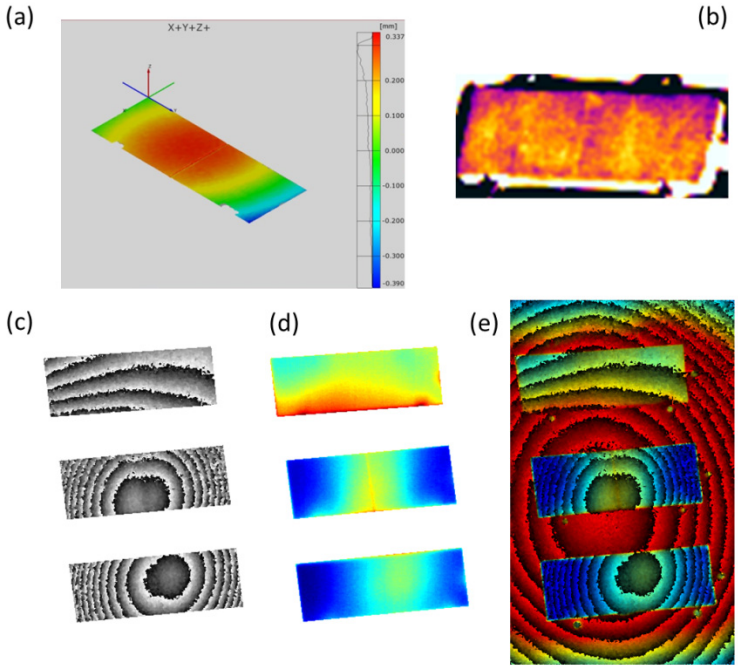

Fig. 9. (a) Deformation measurement by fringe projection, (b) temperature measurement by separate thermographic camera, (c) phase map showing deformation of the three coupons (baseplate is masked), (d) simultaneous temperature variation, (e) hybrid view of deformation and temperature variation showing the baseplate behavior.

6. Conclusion-discussion

We have presented an original application of holography at infrared wavelengths in the LWIR spectral range, which corresponds to the domain of radiation of objects at room temperature. We use CO_2 lasers combined to the digital recording of holograms on microbolometer arrays. The image-plane digital holography configuration (or similarly electronic speckle pattern interferometry) allows obtaining the thermal image of the object and its hologram simultaneously in each pixel. The applications envisaged in our works are related to nondestructive testing in the field of experimental mechanics where full-field monitoring of deformation and temperature variations is needed.

The concept (a single combined sensor) and its advantages have been demonstrated on two examples where deformations were provoked by heating composite structures or coupons. Although these examples are related to experimental mechanics, this technique could be applied to other fields where temperature and optical path differences (related to shape or refractive index changes) need to be measured (fluid mechanics, life sciences,…).

The innovative application presented here is only feasible with digital holography at thermal infrared wavelengths. The latter has already shown other tremendous possibilities in safety [11] that holography at shorter wavelengths cannot achieve. Very recently the demonstration of infrared quantum cascade lasers applied to digital holography [23] further comforts the idea that LWIR holography is an exciting field to explore which certainly will gain from ongoing advances in both sources and camera technologies.

Acknowledgments

These works are funded by the FP7 European project FANTOM (ACP7-GA-2008-213457).

#222130 - $15.00 USD Received 1 Sep 2014; revised 6 Oct 2014; accepted 7 Oct 2014; published 13 Oct 2014